

# kNN-Res: Residual Neural Network with kNN-Graph Coherence for Point Cloud Registration

Muhammad S. Battikh<sup>1</sup>, Artem Lensky<sup>2</sup>, Dillon Hammill<sup>3</sup>, Matthew Cook<sup>4</sup>

<sup>1</sup> New Mexico State University, NM, USA

msbattikh@nmsu.edu

<sup>2</sup> University of New South Wales, ACT, Australia

University of Sydney, NSW, Australia

a.lenskiy@unsw.edu.au, artem.lensky@sydney.edu.au

<sup>3</sup> Australian National University, Australia

dillon.hammill@anu.edu.au

<sup>4</sup> University of Cambridge, UK

mc2386@cam.ac.uk

**Abstract.** In this paper, we present a method based on a residual neural network for point set registration that preserves the topological structure of the target point set. Similar to coherent point drift (CPD), the registration (alignment) problem is viewed as the movement of data points sampled from a target distribution along a regularized displacement vector field. Although the coherence constraint in CPD is stated in terms of local motion coherence, the proposed regularization relies on a global smoothness constraint as a proxy for preserving local topology. This makes CPD less flexible when the deformation is locally rigid but globally non-rigid as in the case of multiple objects and articulate pose registration. A kNN-graph coherence cost and geometric-aware statistical distances are proposed to mitigate these issues. To create an end-to-end trainable pipeline, a simple Jacobian-based cost is introduced as a proxy for the intrinsically discrete kNN-graph cost. We present a theoretical justification for our Jacobian-based cost showing that it is sufficient for the preservation of the kNN-graph of the transformed point set. Further, to tackle the registration of high-dimensional point sets, a constant time stochastic approximation of the kNN-graph coherence cost is introduced. The proposed method is illustrated on several 2-dimensional examples and tested on high-dimensional flow cytometry datasets where the task is to align two distributions of cells whilst preserving the kNN-graph in order to preserve the biological signal of the transformed data.

**Keywords:** point set registration · data topology · optimal transport · kNN.

## 1 Introduction

Point set registration is a widely studied problem in the field of computer vision. The problem involves aligning a deformed target set of  $d$ -dimensional points to another reference point set by applying a constrained transformation. This alignment allows for improved comparison and analysis of the two sets of points and is used in a variety of fields including object tracking, body shape modelling, human pose estimation, and removal of batch effects in biological data [12,33,31,28].

Point set registration techniques are typically categorized based on two main properties, first, whether the technique is a correspondence-based or a correspondence-free technique, and second, whether the estimated transformation is rigid or non-rigid. Correspondence-based techniques require the availability of correspondence information (e.g. labels) between the two point sets, while correspondence-free, sometimes called simultaneous pose and correspondence registration techniques, do not require such information and therefore the problem is considered significantly more difficult. Rigid registration techniques are also generally simpler. A rigid transformation is an isometric transformation that preserves the pairwise distance between points, and such transformation is typically modeled as a combination of rotation and translation. Several rigid registration techniques have been proposed in [2,1,27,5,21,20,15]. Assuming the transformation is rigid, however, makes the types of deformations that could be handled quite limited. Non-rigid transformations allow for more flexibility; however, this makes the problem ill-posed, as there are an infinite number of transformations that could align two point sets, as such, non-rigid registration techniques employ additional constraints. In the next section, we formulate the non-rigid registration problem and introduce the relevant terminology.

### 1.1 Problem Formulation

Given a reference set  $\mathbf{R} = \{\mathbf{x}_1, \dots, \mathbf{x}_n\}$  and a target set  $\mathbf{T} = \{\mathbf{y}_1, \dots, \mathbf{y}_m\}$ , generated by two unknown probability distributions, where  $\mathbf{x}, \mathbf{y} \in \mathbb{R}^d$ , or in matrix form  $X \in \mathbb{R}^{n \times d}$  and  $Y \in \mathbb{R}^{m \times d}$ ; the goal of an alignment method is to estimate a transformation  $\phi$  parameterized by  $\theta$  that preserves the local topology of  $\mathbf{T}$  such that  $\hat{\theta} = \arg \min_{\theta} D(\phi(\mathbf{Y}; \theta), \mathbf{X})$ , where  $D$  is a statistical distance measuring the difference between the two probability distributions. The notion of local topology of a point set is captured by its  $k$ -Nearest Neighbour graph ( $k\text{NN}_g$ ). A  $k\text{NN}$ -graph for set  $\mathbf{T}$  is a directed graph such that there is an edge from node  $i$  to  $j$  if and only if  $\mathbf{y}_j$  is among  $\mathbf{y}_i$ 's  $k$  most similar items in  $\mathbf{T}$  under some similarity measure  $\rho$ . Thus, the aforementioned estimation problem is subject to the constraint:  $k\text{NN}_g(\phi(\mathbf{Y}; \theta)) = k\text{NN}_g(\mathbf{Y})$ .

### 1.2 Limitations of Existing Approaches

A classic example of constraining the alignment transformation is CPD [22] and its extensions [23,11,10]. CPD uses a Gaussian Mixture Model to induce a displacement field from the target to source points and uses local motion coherence to constrain the field such that nearby target points move together. CPD achieves this however via a global smoothing constraint which makes it locally inflexible and therefore unsuitable for articulated deformations in 3D human data, scenes with multiple objects, and biological data [6].

In this work, we introduce a Jacobian orthogonality loss and show that it is a sufficient condition for preserving the  $k\text{NN}$  graph of the data. Jacobian orthogonality introduced as a penalty  $|\mathbf{J}_{\mathbf{Y}}^{\top} \mathbf{J}_{\mathbf{Y}} - \mathbf{I}_d|$  where  $\mathbf{J}_{\mathbf{Y}}$  is the Jacobian matrix at a point  $\mathbf{Y}$  and  $\mathbf{I}_d$  is the  $d \times d$  identity matrix. The penalty has been proposed in other contexts as well, such as unsupervised disentanglement [32] and medical image registration [26,18].

In [26], the finite difference method is employed to compute the Jacobian penalty for the B-splines warping transformation, and mutual information of corresponding voxel intensities is used as the similarity measure. Instead of using finite difference for the Jacobian penalty, which produces a numerical approximation of first-order derivatives, the authors of [18] derive an analytical derivative specific to the multidimensional B-splines case. Such approaches however are limited to low dimensions by the nature of the transformations used, the way in which the Jacobian penalty is computed, and their proposed similarity measures. To address these limitations, we use Hutchinson’s estimator [32,13] for fast computation of the Jacobian loss for high-dimensional point sets, a scalable ResNet [9] architecture as our warping transformation, and geometry-aware statistical distances. It is worth noting that Moment-matching ResNet(MM-Res) [28] uses a similar ResNet architecture with RBF kernel maximum-mean discrepancy as its similarity measure [7,8], however, no topological constraints are provided to preserve the topological structure of the transformed data nor to limit the nature of the learned transformation as shown in Figure 1. Additionally, while maximum-mean discrepancy is a geometry-aware distance, such a kernel blinds the model to details smaller than its standard deviation, and the networks’ gradient suffers from the well-known vanishing gradient problem. We address these limitations by incorporating Sinkhorn divergence into our framework [25].

## 2 Proposed Method

In our work, the transformation  $\phi$  is modelled as a residual mapping and the constrained registration problem is formulated as a relaxed minimization problem using the following loss:

$$\mathcal{L}(\theta) = \mathcal{L}_1 + \lambda \mathcal{L}_2$$

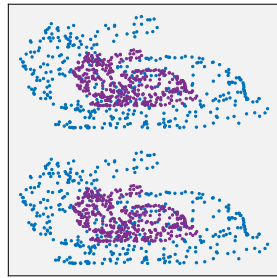
where the alignment loss  $\mathcal{L}_1$  is a geometry-aware statistical distance  $D(\phi(\mathbf{Y}; \theta), \mathbf{X})$ ,  $\lambda$  is a hyperparameter, and  $\mathcal{L}_2$  is the topology-preserving loss:

$$\mathcal{L}_2 = \frac{1}{m} \sum_{\mathbf{y} \in \mathbf{T}} |\mathbf{J}_{\mathbf{y}}^{\top} \mathbf{J}_{\mathbf{y}} - \mathbf{I}_d| \quad (1)$$

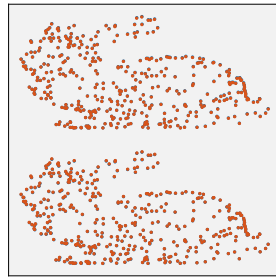
where  $\mathbf{J}_{\mathbf{y}}$  is the Jacobian matrix of the transformation at point  $\mathbf{y}$ . Fig. 1 qualitatively shows the effect of  $\mathcal{L}_2$  and in the next sections we prove that the orthogonality of the Jacobian matrix is indeed a sufficient condition to preserve the kNN graph of  $\mathbf{T}$ . In order to measure the misalignment between the two sets, we employ two geometry-aware statistical distances, namely, Sinkhorn divergences, and maximum-mean discrepancy (MMD) [7]. The Sinkhorn divergence is a computationally efficient approximation of the Wasserstein distance in high dimensions and is defined as follows:

$$\mathcal{L}_1(\theta) = S_{\epsilon}(\alpha, \beta) = \text{OT}_{\epsilon}(\alpha, \beta) - \frac{1}{2}(\text{OT}_{\epsilon}(\alpha, \alpha) + \text{OT}_{\epsilon}(\beta, \beta)) \quad (2)$$

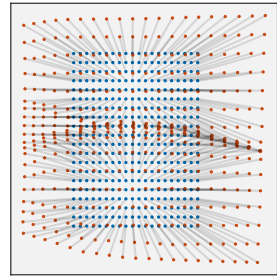
where  $\text{OT}_{\epsilon}$  is the entropic-regularized optimal transport with  $\mathcal{L}_2$ -norm cost, and  $\alpha$  and  $\beta$  are measures over reference and target distributions respectively. The measures



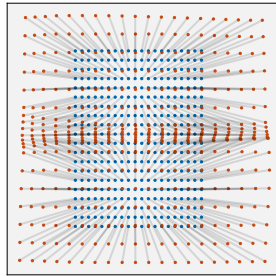
(a) Original(blue) and scaled by a factor of 0.5 bunnies(magenta)



(b) The bunny after being transformed with regularization (red).



(c) The transformation (grid warping) learned without regularization.



(d) The transformation learned (grid warping) with the Jacobian penalty.

Fig. 1: Stanford Bunny example showing the effect of the Jacobian penalty on the learned transformation.

$\alpha$  and  $\beta$  are unknown and are only known via samples from  $\mathbf{R}$  and  $\mathbf{T}$  respectively. [17] show that:  $\lim_{\epsilon \rightarrow 0} S_\epsilon(\alpha, \beta) = \text{OT}(\alpha, \beta)$  and  $\lim_{\epsilon \rightarrow \infty} S_\epsilon(\alpha, \beta) = \frac{1}{2} \text{MDD}_{-C}^2(\alpha, \beta)$ , where  $C$  is the kernel used by MMD. Despite this interpolation property, we still maintain an efficient standalone MMD distance:

$$\text{MMD}(\alpha, \beta) := \frac{1}{2} \int_{X^2} k(\mathbf{x}, \mathbf{y}) d\zeta(\mathbf{x}) d\zeta(\mathbf{y}) \quad (3)$$

with  $k(\mathbf{x}, \mathbf{y})$  being a kernel, that we choose to be Gaussian. This version is used for datasets where MMD is known to perform better, thus avoiding costly indirect computation of MMD via Sinkhorn divergence.

## 2.1 Alignment Transformation

A residual type of mapping is chosen as the aligning transformation. In its most general form, the map is given by  $\phi(\mathbf{x}; \theta) = \mathbf{x} + \delta(\mathbf{x}; \theta)$ , where  $\delta$  is a learned function. For simplicity, we chose this function to be represented by a multilayer perceptron (MLP) with `LeakyRelu` activation functions.

The residual type of mapping has been chosen for two reasons: Firstly, by biasing  $\theta$  to have small values via weight decay or by initializing the output layer of the MLP with small values (e.g. sampled from Gaussian with zero mean and small standard deviation); the contribution of  $\delta(\mathbf{x}; \theta)$  to the final transformation becomes small, which in turn would make  $\phi(\mathbf{x}; \theta)$  close to the identity. Secondly, since we follow a CPD-like framework, by viewing the alignment transformation as a regularized movement (drift) of data points along a displacement vector field  $\mathcal{F}$ , it becomes mathematically and computationally convenient to have  $\phi(\mathbf{x}; \theta)$  as a ResNet identity block. In such a case, the displacement vector is the difference between the final position  $\phi(\mathbf{x} : \theta)$  (transformed point) and the initial position (data point)  $\mathbf{x}$  such that  $\mathcal{F}(\mathbf{x}) = \phi(\mathbf{x} : \theta) - \mathbf{x} = \delta(\mathbf{x} : \theta)$ , and therefore, only  $\delta(\mathbf{x} : \theta)$  has to be taken care of, instead of  $\phi(\mathbf{x} : \theta) - \mathbf{x}$ , absent skip connection.

## 2.2 Jacobian Loss via Finite Difference

Given a vector-valued function  $\mathcal{F} : \mathbb{R}^d \rightarrow \mathbb{R}^d$ , a data batch  $\mathbf{X} \in \mathbb{R}^{m \times d}$ , and the Jacobian  $\mathbf{J}_{\mathbf{X}}$  of  $\mathcal{F}$  at each of  $m$  points, which constitutes a  $\mathbb{R}^{m \times d \times d}$  tensor, it is possible to compute  $\mathbf{J}_{\mathbf{X}}$  analytically using auto-differentiation modules, however, such computation is highly inefficient, thus, we resort to numerical approximation.

Given a  $d$ -dimensional vector  $\mathbf{x} = [x_1, \dots, x_d]^\top$ , the partial first derivative of  $\mathcal{F}$  with respect to  $x_i$  is:

$$\frac{\partial \mathcal{F}}{\partial x_i} = \lim_{\epsilon \rightarrow 0} \frac{\mathcal{F}(\mathbf{x} + \epsilon \mathbf{e}_i) - \mathcal{F}(\mathbf{x})}{\epsilon}, \quad (4)$$

where  $\mathbf{e}_i$  is a standard basis vector (i.e. only the  $i$ th component is 1 and the rest are zeros). This derivative could be approximated numerically using a small  $\epsilon$ . The Jacobian matrix  $\mathbf{J}_{\mathbf{x}}$  is simply  $[\frac{\partial \mathcal{F}}{\partial x_1}, \dots, \frac{\partial \mathcal{F}}{\partial x_d}]$ . To ensure the orthogonality of the Jacobian at  $\mathbf{X}$ , we minimize the following loss:

$$\mathcal{L}_2 = \frac{1}{m} \sum_{\mathbf{x} \in \mathbf{X}} |\mathbf{J}_{\mathbf{x}}^\top \mathbf{J}_{\mathbf{x}} - \mathbf{I}_d| \quad (5)$$

### 2.3 Orthogonal Jacobian Preserves kNN Graph

In this section, we show that the orthogonality of the Jacobian matrix evaluated at data points is a sufficient condition for preserving the kNN graph of the data. A vector-valued function  $\mathcal{F} : \mathbb{R}^n \rightarrow \mathbb{R}^n$  preserves the kNN graph of data points  $\mathbf{X} \in \mathbb{R}^n$  if, for every two points  $\mathbf{v}$  and  $\mathbf{w}$  that are in some small  $\epsilon$ -neighborhood of  $\mathbf{u}$  containing  $k$  points, the following holds:

$$\|\mathbf{u} - \mathbf{v}\|_2^2 < \|\mathbf{u} - \mathbf{w}\|_2^2 \rightarrow \|\mathcal{F}(\mathbf{u}), \mathcal{F}(\mathbf{v})\|_2^2 < \|\mathcal{F}(\mathbf{u}), \mathcal{F}(\mathbf{w})\|_2^2, \quad (6)$$

where  $\|\cdot\|_2^2$  is the squared Euclidian distance. Without loss of generality, we choose two points  $\mathbf{w}, \mathbf{v}$  that lie in  $\epsilon$ -neighborhood of point  $\mathbf{u}$  and linearize the vector field  $\mathcal{F}$  around point  $\mathbf{u}$  such that:

$$\mathcal{F}(\mathbf{x}; \mathbf{u}) \approx \mathcal{F}(\mathbf{u}) + \mathbf{J}_{\mathbf{u}}(\mathbf{x} - \mathbf{u}), \quad (7)$$

where  $\mathbf{J}_{\mathbf{u}}$  is the Jacobian matrix evaluated at point  $\mathbf{u}$  with step size  $\epsilon$ . The squared distance of  $\mathbf{u}$  and  $\mathbf{v}$  is:

$$\|\mathbf{u} - \mathbf{v}\|_2^2 = (\mathbf{u} - \mathbf{v})^\top (\mathbf{u} - \mathbf{v}) = \sum_i^n (\mathbf{u}_i - \mathbf{v}_i)^2 \quad (8)$$

Similarly, the squared distance between  $\mathcal{F}(\mathbf{u}; \mathbf{u})$  and  $\mathcal{F}(\mathbf{v}; \mathbf{u})$  computes as follows

$$\begin{aligned} & \|\mathcal{F}(\mathbf{u}; \mathbf{u}) - \mathcal{F}(\mathbf{v}; \mathbf{u})\|_2^2 \\ &= (\mathcal{F}(\mathbf{u}; \mathbf{u}) - \mathcal{F}(\mathbf{v}; \mathbf{u}))^\top (\mathcal{F}(\mathbf{u}; \mathbf{u}) - \mathcal{F}(\mathbf{v}; \mathbf{u})) \\ &= (\mathcal{F}(\mathbf{u}) - \mathcal{F}(\mathbf{u}) - \mathbf{J}_{\mathbf{u}}(\mathbf{v} - \mathbf{u}))^\top \\ & \quad (\mathcal{F}(\mathbf{u}) - \mathcal{F}(\mathbf{u}) - \mathbf{J}_{\mathbf{u}}(\mathbf{v} - \mathbf{u})) \\ &= (\mathbf{J}_{\mathbf{u}}(\mathbf{v} - \mathbf{u}))^\top (\mathbf{J}_{\mathbf{u}}(\mathbf{v} - \mathbf{u})) \\ &= (\mathbf{v} - \mathbf{u})^\top \mathbf{J}_{\mathbf{u}}^\top \mathbf{J}_{\mathbf{u}} (\mathbf{v} - \mathbf{u}) \\ &= (\mathbf{v} - \mathbf{u})^\top (\mathbf{v} - \mathbf{u}) \end{aligned} \quad (9)$$

The last step follows from the orthogonality of  $\mathbf{J}_{\mathbf{u}}$  i.e. ( $\mathbf{J}_{\mathbf{u}}^\top \mathbf{J}_{\mathbf{u}} = \mathbf{I}$ )

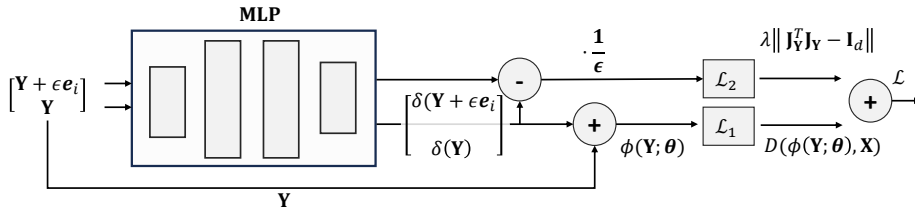


Fig. 2: Training pipeline for the proposed alignment.

## 2.4 Training

The training process (alg. 1) starts by sampling points from  $\mathbf{R}$  and  $\mathbf{T}$  and constructing two matrices  $\mathbf{X}$  and  $\mathbf{Y}$ . The matrix  $\mathbf{Y}$  is then fed to the model  $\phi(\mathbf{Y})$  and the alignment loss  $\mathcal{L}_1$  is computed by either using the Sinkhorn divergence(2) or MMD(3). For  $\mathcal{L}_2$ , we use the finite difference to estimate the Jacobian for each input data point by taking a small step in the direction of each standard basis vector  $e_i$  and compute the mean of the Jacobian deviation from orthogonality. Finally, we compute the combined loss  $\mathcal{L} = \mathcal{L}_1 + \lambda\mathcal{L}_2$  and use backpropagation to update the network weights until convergence. A visualization of the training pipeline is shown in figure 2.

---

### Algorithm 1: Training kNN-Res

---

**Input:**  $\mathbf{R}$ , and  $\mathbf{T}$  pointsets, blurring factor  $\sigma$ , step size  $\epsilon$ , regularisation  $\lambda$ , and batch size  $b$ ;  
**Output:** Trained model ▷ Sample mini-batches of size  $b$  from  $\mathbf{R}$  and  $\mathbf{T}$   
**while**  $(\mathbf{X}, \mathbf{Y}) \in (\mathbf{R}, \mathbf{T})$  *until convergence* **do**  
   $\phi(\mathbf{Y}) \leftarrow \mathbf{Y} + \delta(\mathbf{Y})$ ;  
  **if** *loss* == "sinkhorn" **then**  
     $\mathcal{L}_1 = \mathcal{S}(\mathbf{X}, \phi(\mathbf{Y}); \sigma^2)$ ;  
  **else**  
     $\mathcal{L}_1 = \text{MMD}(\mathbf{X}, \phi(\mathbf{Y}); \sigma^2)$ ;  
     $\mathbf{J}_{\mathbf{Y}}[i, :] = \frac{\delta(\mathbf{Y} + \epsilon \mathbf{e}_i) - \delta(\mathbf{Y})}{\epsilon}$ ;  
     $\mathcal{L}_2 = \frac{1}{m} \sum_{\mathbf{y} \in \mathbf{Y}} |\mathbf{J}_{\mathbf{y}}^{\top} \mathbf{J}_{\mathbf{y}} - \mathbf{I}_d|$ ;  
     $\mathcal{L} = \mathcal{L}_1 + \lambda\mathcal{L}_2$ ;  
▷ backpropagation step  
  Minimize( $\mathcal{L}$ );

---

## 2.5 Stochastic Approximation of Orthogonal Jacobian Loss

Computing the Jacobian using finite difference is considered efficient for low-dimensional point sets, however, the computational cost increases linearly with increasing data dimensionality. Thus, an approximate estimate with the constant computational cost is introduced.

Given a vector-valued function  $\mathcal{F}$ , and a sample  $\mathbf{x}$ , the following is minimized:

$$\mathcal{L}_{\mathbf{J}}(\mathcal{F}) = |\mathbf{J}^{\top} \mathbf{J} \circ (\mathbf{1} - \mathbf{I})|_2 = \sum_{i \neq j} \frac{\partial \mathcal{F}_i}{\partial x_j} \frac{\partial \mathcal{F}_j}{\partial x_i} \quad (10)$$

Following [32,13], the Hutchinson's estimator of  $\mathcal{L}_{\mathbf{J}}(\mathcal{F})$  can be approximated as such:

$$\mathcal{L}_{\mathbf{J}}(\mathcal{F}) = \text{var}_r(r_{\epsilon}^{\top} (\mathbf{J}^{\top} \mathbf{J}) r_{\epsilon}) = \text{var}_r((\mathbf{J} r_{\epsilon})^{\top} (\mathbf{J} r_{\epsilon})) \quad (11)$$

where  $r_{\epsilon}$  denotes a scaled Rademacher vector (with equal probability each entry is either  $-\epsilon$  or  $+\epsilon$ ) where  $\epsilon > 0$  is a hyperparameter that controls the granularity of the

first directional derivative estimate and  $\text{Var}_r$  is the variance. It is worth noting that this does not guarantee orthonormality, only orthogonality. In practice, however, we find that such an estimator produces results comparable to those of the standard finite difference method.

### 3 Experiments

In order to evaluate the proposed point set registration method we experimented with several synthesized dataset, introduced by Chui-Rangarajan in [3,34,19], and flow cytometry data used in [28]. The Chui-Rangarajan synthesized dataset is comprised of two shapes: a fish shape, and a Chinese character shape. Each shape is subjected to 5 increasing levels of deformations using an RBF kernel, and each deformation contains 100 different samples. The samples are generated using different RBF coefficients which are sampled from a zero-mean normal distribution with standard deviation  $\sigma$ , whereby increasing  $\sigma$  leads to generally larger deformation.

#### 3.1 Results on 2D Data

The root-mean-squared error defined as  $\text{error} = \sqrt{\frac{1}{m} \sum_{i=0}^m (\hat{y}_i - y_i)^2}$  is computed between the transformed  $\hat{y}_i$  and the ground truth  $y_i$  point sets, the latter available in the Chui-Rangarajan synthesized dataset.

It is important to note that such ground-truth correspondence is absent during training time and is only available during test time. We report results for our kNN-Res as well as for MM-Res[28], CPD [22], TRS-RPM [3], RPM-LNS [19], and GMM-REG [14] over 5 deformation levels and 100 samples per level. Figures 3a and 3b show results for the tested models for the Chinese character, and Fish datasets respectively. We notice that after a certain level of non-rigid deformation, MM-Res is unable to converge. For our kNN-Res, we set the finite difference step size to  $\epsilon = .005$ , regularization factor to  $\lambda = 10^{-5}$ , blur(interpolation) parameter between OT and MMD to  $\sigma = .001$  and the number of units in the two hidden layers is set to 50. The initial learning rate is 0.01 for the ADAM [16] optimizer and uses a reduce-on-plateau scheduler with a reduction factor of 0.7 whereas the minimum learning rate is set to  $5 \times 10^{-5}$ . To quantitatively assess neighbourhood preservation we use the hamming loss  $\mathcal{L}_H$  to estimate the difference between the kNN graph before and after transformation:  $\mathcal{L}_H = \sum_{i=0}^m \sum_{j=0}^m I(\hat{p}_{i,j}^k \neq p_{i,j}^k)$  where  $p_{i,j}^k$  is the  $i,j$  element of the kNN graph matrix before transformation,  $\hat{p}_{i,j}^k$  is the corresponding element after transformation, and  $I$  is the indicator function. Figures 4 show the difference in neighborhood preservation between MM-Res (MMD alignment without regularization) and our kNN-Res for the Chinese character, and Fish datasets, respectively, for three different levels of deformations. It should be noted that MM-Res completely failed for large deformations (level >3).

Moreover, despite the additional topology regularization term, our kNN-Res model generally incurred smaller alignment errors and was able to converge under large deformation levels.



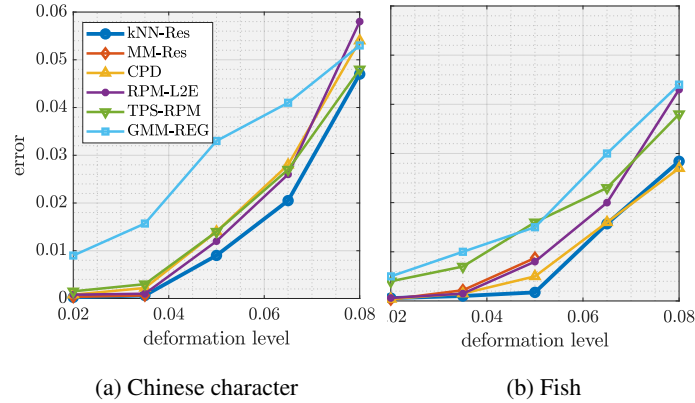


Fig. 3: Evaluation metrics

### 3.2 Results on High-Dimensional CyTOF Data

Cytometry by time of flight (CyTOF) provides a means for quantifying multiple cellular components; however, it is susceptible to the so-called batch effect problem, where systematic non-biological variations during the measurement process result in distributional shifts of otherwise similar samples.

This effect breaks the intra-comparability of samples which is a crucial component of downstream tasks such as disease diagnosis and typically requires the intervention of human experts to remove these batch effects. The CyTOF dataset used in our experiments was curated by Yale New Haven Hospital. There are two patients, and two conditions were measured on two different days. All eight samples have 25 markers each representing a separate dimension, and a range of cells (points) between 1800 to 5000 cells per sample. The split is done such that samples collected on day 1 are the target, and samples collected on day 2 are the reference, resulting in four alignment experiments. We follow the exact preprocessing steps described in [28]. To adjust the dynamic range of samples, a standard pre-preprocessing step of CyTOF data is to apply a log transformation [4]. Additionally, CyTOF data typically contains a large number of zero values (40%) due to instrumental instability which are not considered biological signals. Thus, a denoising autoencoder (DAE) is used to remove these zero-values [30]. The Encoder of the DAE is comprised of two fully-connected layers with ReLU activation functions. The decoder (output) is a single linear layer, with no activation function. All layers of the DAE have the same number of neurons as the dimensionality of the data. Next, each cell is multiplied by an independent Bernoulli random vector with probability 0.8, and the DAE is trained to reconstruct the original cell using the Mean Squared Error loss. Furthermore, the DAE is optimized via RMSprop and weight decay regularization. The zero values in both reference and target are then removed using the trained DAE. Finally, each feature in both target and reference samples is independently standardized to have a zero-mean and unit variance. For our kNN-Res model, we set  $\epsilon = 0.05$ ,  $\lambda = 0.1$ ,  $\sigma = 0.04$ , and  $k = 5$  for Hutchinson’s estimator, and the number

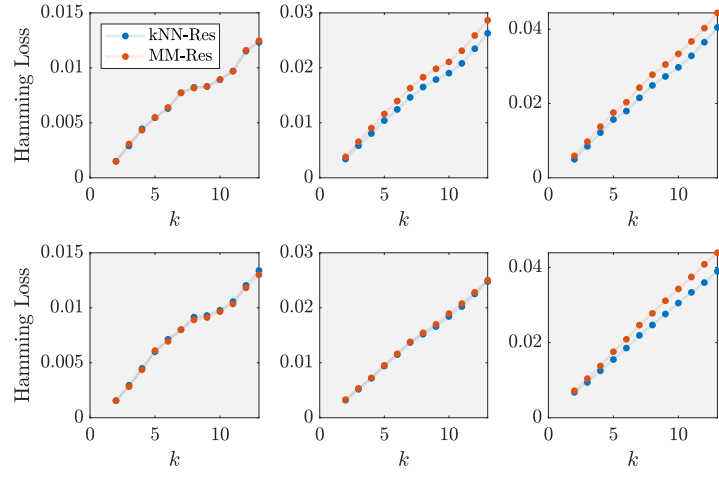
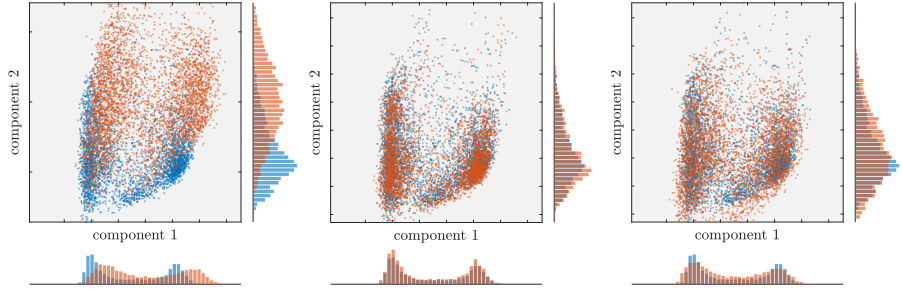
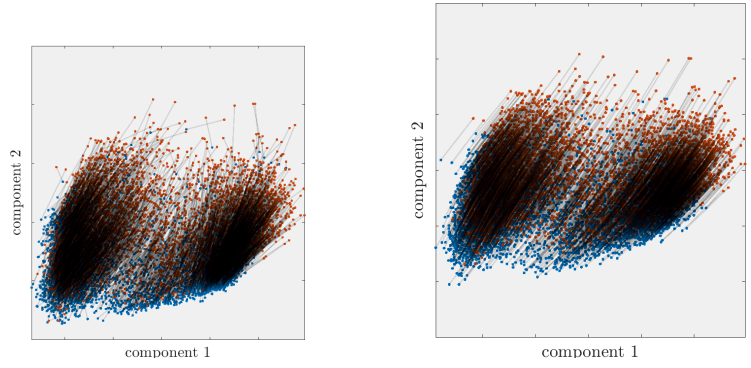


Fig. 4: Hamming loss for the following levels of deformations: (left) level 1, (mid) level 2, (right) level 3. Top row: Fish shape. Bottom row: Chanese character.



(a) Unaligned distributions (b) Aligned w/o const. ( $\lambda = 0$ ) (c) Aligned w/ const. ( $\lambda = 1$ )



(d) Alignment w/o geom. cont. (i.e.  $\lambda = 0$ ) (e) Alignment w/ geom. cont. (i.e.  $\lambda = 1$ )

Fig. 5: The blue/red dots are 1st/2nd components of reference (patient #2, day 2) and the target (patient #2, day 1). The alignment was performed in the 25d CyTOF space.

of units in the two hidden layers are set to 50. As previously, the initial learning rate is set to 0.01 for the ADAM optimizer and uses a reduce-on-plateau scheduler with a reduction factor of .7, with the minimum learning rate of  $5 \times 10^{-5}$ . Fig. 5 shows the first two principal components of data before and after alignment using two kNN-Res models with different lambdas. Although the two samples appear less aligned when using a large  $\lambda$ , this comes with the benefit of preserving the topology of the data as shown by the learned transformation in Fig. 5e where points (cells) are moved in a coherent way compared to fig. 5d.

The benefits of topologically preserving normalization become clearer when examining the marginals in Fig. 6. In this experiment, we trained five models with five different lambdas ranging from 0 to 1. It is clear that having a small  $\lambda$  favours alignment over faithfulness to the original distribution, however, increasing  $\lambda$  preserves the shape of the original data after transformation, which is desirable in biological settings. By preserving the kNN graph, our method ensures that key biological signals are not lost during the alignment process, mitigating the risk of introducing non-biological variability. Additionally, the demonstrated scalability of the model to high-dimensional datasets suggests potential for its use in other fields beyond biology.

## 4 Discussion

### 4.1 Parameters Selection

The proposed method has three main hyperparameters, namely:  $\sigma$ ,  $\epsilon$ , and  $\lambda$ . In the case of Sinkhorn divergence,  $\sigma > 0$  is the blur (interpolation) parameter between OT and MMD, with a default value of 0.01 for datasets that lie in the first quadrant of the unit hypercube (minmax normalized data). Decreasing  $\sigma$  has the effect of solving for an exact OT, which typically produces very accurate registration; however, this comes at a slower convergence cost. In the cases where it is more advantageous to use MMD,  $\sigma$  represents the standard deviation of the Gaussian kernel.  $\epsilon > 0$  represents the finite difference step size and controls the radius of topology preservation around each point. It is worth noting that a large epsilon value that covers all data tends to produce globally isomorphic transformations. As shown in 6,  $\lambda > 0$  is simply a regularization parameter that prioritizes regularization over alignment and is typically less than 0.01.

### 4.2 Implications

Point set registration methods are typically used for problems in computer vision to align point clouds produced by either stereo vision or by Light Detection and Ranging devices (e.g. Velodyne scanner) for instance to stitch scenes and align objects. These datasets are usually of 2 or 3 dimensions and hence such methods have limited exposure to high-dimensional datasets. Biological data, on the other hand, is usually of high dimension and hence methods from point-set registration do not directly translate to biological data. The proposed method in this study was tested on a 25-dimensional CyTOF dataset. However, in flow and mass cytometry, data could easily go beyond 50 dimensions (markers). For instance, methods that combine protein marker detection

with unbiased transcriptome profiling of single cells provide an even higher number of markers in order to achieve a more detailed characterization of cell phenotypes than transcriptome measurements alone [29,24]. Unfortunately, these methods require more sophisticated batch normalization algorithms, since manual gating and normalization using marginal distributions, which is currently commonly applied, become infeasible. It is worth mentioning that even while experts are making sure that the marginal distributions are aligned, there is still no guarantee that the samples are aligned in the higher-dimensional space. Moreover, the alignment might result in such nonlinear and nonsmooth transformations that break biological relationships or introduce nonexisting biological variabilities. The proposed method mitigates these issues and guarantees smooth transformations.

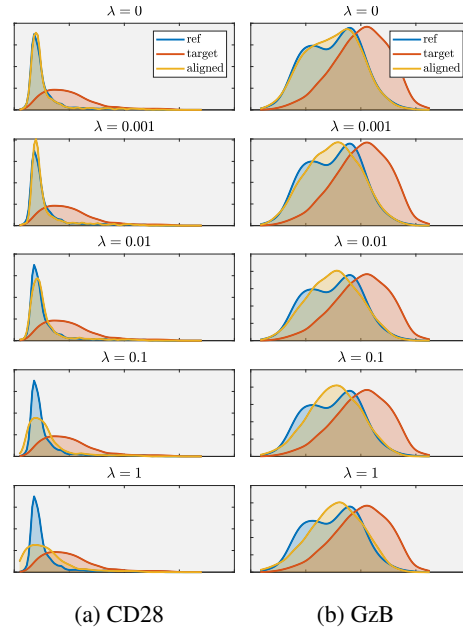


Fig. 6: Marginals density plot for markers CD28 and GzB under varying regularization  $\lambda$ . Each subplot shows reference (blue), target (red), and aligned (orange).

## 5 Conclusion and Future Work

This paper presents a simple but scalable framework for point-cloud registration. At its core, it consists of three components, namely (a) residual-based transformation as a parametrized displacement field, (b) Jacobian penalty as a topology-preserving loss, and (c) Sinkhorn Divergence as a sample-based, geometry-aware statistical distance. Additionally, by incorporating Hutchinson’s estimator for the Jacobian loss, we show

that our model is easily extensible to high dimensions with constant complexity. One future direction is to incorporate local or partial matching using modified alignment losses such as the Gromov-Wasserstein distance. This should lead to a much more robust solution than global matching, especially in the case of outliers and missing objects.

## References

1. Besl, P.J., McKay, N.D.: Method for registration of 3-d shapes. In: Sensor fusion IV: control paradigms and data structures. vol. 1611, pp. 586–606. Spie (1992)
2. Brown, L.G.: A survey of image registration techniques. *ACM computing surveys (CSUR)* **24**(4), 325–376 (1992)
3. Chui, H., Rangarajan, A.: A new point matching algorithm for non-rigid registration. *Computer Vision and Image Understanding* **89**(2-3), 114–141 (2003)
4. Finck, R., Simonds, E.F., Jager, A., Krishnaswamy, S., Sachs, K., Fantl, W., Pe’er, D., Nolan, G.P., Bendall, S.C.: Normalization of mass cytometry data with bead standards. *Cytometry Part A* **83**(5), 483–494 (2013)
5. Fitzgibbon, A.W.: Robust registration of 2d and 3d point sets. *Image and Vision Computing* **21**(13-14), 1145–1153 (2003)
6. Ge, S., Fan, G., Ding, M.: Non-rigid point set registration with global-local topology preservation. In: *Proceedings of the IEEE Conference on Computer Vision and Pattern Recognition Workshops*. pp. 245–251 (2014)
7. Gretton, A., Borgwardt, K., Rasch, M., Schölkopf, B., Smola, A.: A kernel method for the two-sample-problem. *Advances in Neural Information Processing Systems* **19** (2006)
8. Gretton, A., Borgwardt, K.M., Rasch, M.J., Schölkopf, B., Smola, A.: A kernel two-sample test. *The Journal of Machine Learning Research* **13**(1), 723–773 (2012)
9. He, K., Zhang, X., Ren, S., Sun, J.: Deep residual learning for image recognition. In: *Proceedings of the IEEE Conference on Computer Vision and Pattern Recognition*. pp. 770–778 (2016)
10. Hirose, O.: Acceleration of non-rigid point set registration with downsampling and gaussian process regression. *IEEE Transactions on Pattern Analysis and Machine Intelligence* **43**(8), 2858–2865 (2020)
11. Hirose, O.: A bayesian formulation of coherent point drift. *IEEE Transactions on Pattern Analysis and Machine Intelligence* **43**(7), 2269–2286 (2020)
12. Huang, X., Mei, G., Zhang, J., Abbas, R.: A comprehensive survey on point cloud registration. *arXiv preprint arXiv:2103.02690* (2021)
13. Hutchinson, M.F.: A stochastic estimator of the trace of the influence matrix for laplacian smoothing splines. *Communications in Statistics-Simulation and Computation* **18**(3), 1059–1076 (1989)
14. Jian, B., Vemuri, B.C.: Robust point set registration using gaussian mixture models. *IEEE Transactions On Pattern Analysis and Machine Intelligence* **33**(8), 1633–1645 (2010)
15. Khoo, Y., Kapoor, A.: Non-iterative rigid 2d/3d point-set registration using semidefinite programming. *IEEE Transactions on Image Processing* **25**(7), 2956–2970 (2016)
16. Kingma, D.P., Ba, J.: Adam: A method for stochastic optimization. *arXiv preprint arXiv:1412.6980* (2014)
17. Léonard, C.: A survey of the schrodinger problem and some of its connections with optimal transport. *arXiv preprint arXiv:1308.0215* (2013)
18. Loeckx, D., Maes, F., Vandermeulen, D., Suetens, P.: Nonrigid image registration using free-form deformations with a local rigidity constraint. In: *Medical Image Computing and Computer-Assisted Intervention–MICCAI 2004: 7th International Conference, Saint-Malo, France, September 26-29, 2004. Proceedings, Part I* 7. pp. 639–646. Springer (2004)

19. Ma, J., Zhao, J., Tian, J., Tu, Z., Yuille, A.L.: Robust estimation of nonrigid transformation for point set registration. In: Proceedings of the IEEE Conference On Computer Vision and Pattern Recognition. pp. 2147–2154 (2013)
20. Makadia, A., Patterson, A., Daniilidis, K.: Fully automatic registration of 3d point clouds. In: 2006 IEEE Computer Society Conference on Computer Vision and Pattern Recognition (CVPR'06). vol. 1, pp. 1297–1304. IEEE (2006)
21. Mitra, N.J., Gelfand, N., Pottmann, H., Guibas, L.: Registration of point cloud data from a geometric optimization perspective. In: Proceedings of the 2004 Eurographics/ACM SIGGRAPH symposium on Geometry processing. pp. 22–31 (2004)
22. Myronenko, A., Song, X.: Point set registration: Coherent point drift. *IEEE Transactions on Pattern Analysis and Machine Intelligence* **32**(12), 2262–2275 (2010)
23. Myronenko, A., Song, X., Carreira-Perpinan, M.: Non-rigid point set registration: Coherent point drift. *Advances in Neural Information Processing Systems* **19** (2006)
24. Peterson, V.M., Zhang, K.X., Kumar, N., Wong, J., Li, L., Wilson, D.C., Moore, R., McClanahan, T.K., Sadekova, S., Klappenbach, J.A.: Multiplexed quantification of proteins and transcripts in single cells. *Nature Biotechnology* **35**(10), 936–939 (2017)
25. Ramdas, A., García Trillos, N., Cuturi, M.: On wasserstein two-sample testing and related families of nonparametric tests. *Entropy* **19**(2), 47 (2017)
26. Rohlfing, T., Maurer, C.R., Bluemke, D.A., Jacobs, M.A.: Volume-preserving nonrigid registration of mr breast images using free-form deformation with an incompressibility constraint. *IEEE Transactions on Medical Imaging* **22**(6), 730–741 (2003)
27. Rusinkiewicz, S., Levoy, M.: Efficient variants of the icp algorithm. In: Proceedings Third International Conference on 3-D Digital Imaging and Modeling. pp. 145–152. IEEE (2001)
28. Shaham, U., Stanton, K.P., Zhao, J., Li, H., Raddassi, K., Montgomery, R., Kluger, Y.: Removal of batch effects using distribution-matching residual networks. *Bioinformatics* **33**(16), 2539–2546 (2017)
29. Stoeckius, M., Hafemeister, C., Stephenson, W., Houck-Loomis, B., Chattopadhyay, P.K., Swerdlow, H., Satija, R., Smibert, P.: Simultaneous epitope and transcriptome measurement in single cells. *Nature Methods* **14**(9), 865–868 (2017)
30. Vincent, P., Larochelle, H., Bengio, Y., Manzagol, P.A.: Extracting and composing robust features with denoising autoencoders. In: Proceedings of the 25th International Conference on Machine Learning. pp. 1096–1103 (2008)
31. Viola, P., Wells, W.M.: Alignment by maximization of mutual information. In: Proceedings of IEEE International Conference on Computer Vision. pp. 16–23. IEEE (1995)
32. Wei, Y., Shi, Y., Liu, X., Ji, Z., Gao, Y., Wu, Z., Zuo, W.: Orthogonal jacobian regularization for unsupervised disentanglement in image generation. In: Proceedings of the IEEE/CVF International Conference on Computer Vision. pp. 6721–6730 (2021)
33. Weiss, A., Hirshberg, D., Black, M.J.: Home 3d body scans from noisy image and range data. In: 2011 International Conference on Computer Vision. pp. 1951–1958. IEEE (2011)
34. Zheng, Y., Doermann, D.: Robust point matching for nonrigid shapes by preserving local neighborhood structures. *IEEE Transactions on Pattern Analysis and Machine Intelligence* **28**(4), 643–649 (2006)